Torsional Heart Motion in Cone-beam Computed Tomography Reconstruction

Mathias Unberath*†, Katrin Mentl*, Oliver Taubmann*†, Stephan Achenbach‡,
Rebecca Fahrig§, Joachim Hornegger*† and Andreas Maier*†
*Pattern Recognition Laboratory, Friedrich-Alexander Universität Erlangen-Nürnberg
†Graduate School in Advanced Optical Technologies, Friedrich-Alexander Universität Erlangen-Nürnberg
‡University Hospital: Cardiology and Angiology, Friedrich-Alexander Universität Erlangen-Nürnberg
§Radiological Sciences Laboratory, Stanford University

***Abstract*—We study the effects of cardiac twist on phase-resolved cardiac C-arm cone-beam computed tomography reconstruction. First, a numeric, dynamic cardiac phantom is extended with an analytic model describing the heart's twisting motion. Then, phase-resolved reconstructions are calculated using two methods based on ECG-gating and interpolation of the original motion field, respectively.**
We assessed overall reconstruction quality using the correlation of voxel intensities and found it largely unaffected by cardiac twist. We then confined the evaluation to the coronary arteries using the area under precision-recall curves. Decreasing performance at larger twist angles was observed with both methods at both fast and quiet heart phases.
The results indicated that limited angle problems may occur for large twist angles in interventional settings, leading to degraded image quality. However, degradations were subtle and should not affect most practical cases.

I. Introduction

Due to the helical orientation of the left ventricular (LV) myocardial fibers, contraction during systole not only leads to longitudinal and circumferential fiber shorting but also LV twist. The twist axis coincides with the long-axis of the ventricle. Fibers are arranged in a left-handed helix in the subepicardium, resulting in clockwise rotation at the base but counterclockwise rotation at the apex [1]. LV twist has not been studied excessively in the context of X-ray imaging because it cannot be assessed directly using this modality. The coronary arteries, however, follow LV rotation as they are attached to the myocardium. Therefore, LV twist has to be considered in phase-resolved coronary artery reconstruction in contrasted angiography. This study is of particular interest for interventional acquisitions, where rotational motion may lead to limited angle problems resulting in streak artifacts [2]. In order to investigate the effects of cardiac twist on coronary artery reconstruction, we extend the motion field of the XCAT cardiac phantom [3] with a twisting motion model. Then, we evaluate the performance of two phase-resolved cardiac reconstruction algorithms at various twist angles.

II. Material and methods

A. Extensions to the XCAT Heart

The XCAT heart phantom comes with contractive motion in terms of longitudinal and circumferential fiber shortening. As it was partially derived from a tagged MRI scan, LV twist may be included but was not assessed in particular [3]. The phantom is based on an analytic B-spline model that describes the anatomy as well as the motion path [4]. Therefore, it can easily be manipulated by modification of its control points $\mathbf{c}^{(i)} \in \mathbb{R}^3$. The rotation-axis of the torsional heart motion coincides with the long-axis of the left-ventricle, that is assumed linear. Let the long-axis match the z-axis of the reference coordinate system, then the twist angle of control point $\mathbf{c}^{(i)}$ at heart phase $h_r \in [0, 1[$ is linearly interpolated along this axis, yielding

$$\Phi_i(h_r) = \frac{\mathbf{b}_z - \mathbf{c}_z^{(i)}}{\mathbf{b}_z - \mathbf{a}_z}\Phi_{\mathbf{b}}(h_r) - \frac{\mathbf{c}_z^{(i)} - \mathbf{a}_z}{\mathbf{b}_z - \mathbf{a}_z}\Phi_{\mathbf{a}}(h_r), \qquad (1)$$

where $\mathbf{b}$ and $\mathbf{a}$ are the coordinates, and $\Phi_{\mathbf{b}}$ and $\Phi_{\mathbf{a}}$ the corresponding rotation angles of the LV base and apex, respectively. The rotated control points at phase h_r are then given by $\mathbf{c}'^{(i)} = \mathbf{R} \cdot \mathbf{c}^{(i)}$, where R is a rotation matrix describing a rotation of $\Phi_i(h_r)$ around the z-axis. Following Notomi *et al.* we chose $\Phi_{\mathbf{a}} = -2 \cdot \Phi_{\mathbf{b}}$ [5], and $\Phi_{\mathbf{b}}(h_r) = \Phi_{\mathbf{b}}^{\text{max}} \cdot (|2h_r - 1| - 1)$, where $\Phi_{\mathbf{b}}^{\text{max}}$ is the maximal rotation angle at the base. Therefore, the total twist angle is $\Phi^{\text{tot}} = 3 \cdot \Phi_{\mathbf{b}}^{\text{max}}$. Fig. 1 shows the cardiac motion field from $h_r = 0.0$ to $h_r = 0.5$ for a simulation without twist (c.f. Fig. 1a and 1c), and a LV twist of $\Phi^{\text{tot}} = 30°$, i.e. $\Phi_{\mathbf{b}}^{\text{max}} = 10°$ in Fig. 1b and 1d. The resulting difference in coronary artery position at systole is shown in Fig. 2.

B. Phase-resolved Reconstruction

1) ECG-gated interventional cardiac reconstruction: Schwemmer *et al.* proposed a method for the reconstruction of cardiac vasculature from cone-beam rotational angiography using retrospective electrocardiogram-gating (ECG-gating) and deformable 2D-2D registration [6]. We are interested whether LV twist introduces limited-angle problems and hence degrades image quality. Such effects would alter the performance of this method at all stages. Therefore, it is legitimate to confine the method to a restrictively gated initial FDK-type reconstruction at the reference heart phase h_r

$$f_{h_r}(\mathbf{x}) = \sum_{i=1}^{N-2N_{\text{ign}}} \lambda_i(h_r) \cdot \omega_i(\mathbf{x}) \cdot p_i\left(A_i(\mathbf{x})\right), \qquad (2)$$

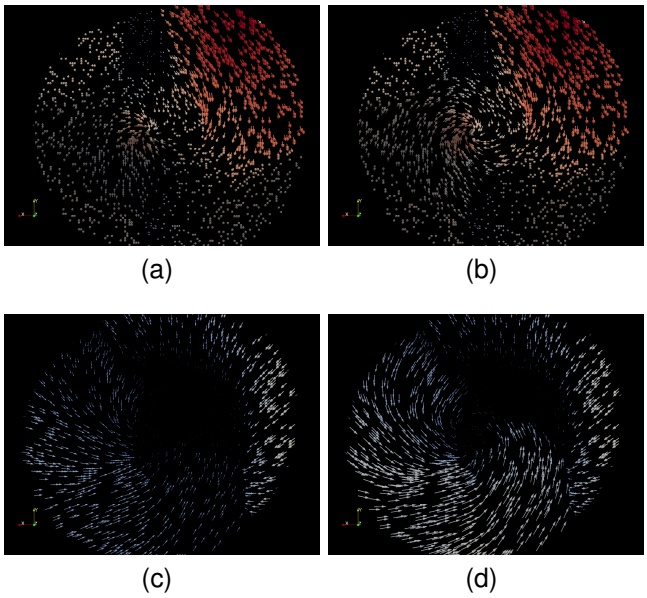

Fig. 1. Basal (Fig. 1a and 1b) and apical (Fig. 1c and 1d) short-axis cross sections of the heart motion field with 0° and 30° twist angle on the left and right hand side, respectively. The strong motion in the upper right corner of the apical slices originates from right ventricular dynamics.

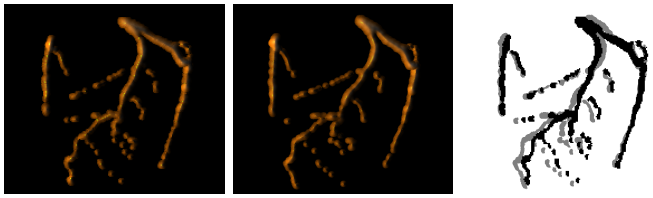

Fig. 2. Volume renderings of the ground-truth coronary arteries at systole ($h_r = 0.5$) using a twist angle of 0° and 30° in Fig. 2a and 2b, respectively. Fig. 2c illustrates differences between 2a (black) and 2b (gray) for emphasis.

where N is the number of projections, $\omega_i(\mathbf{x})$ are distance weights, $p_i(\mathbf{u})$ are the filtered, and cosine- and redundancy-weighted projections at detector coordinate $\mathbf{u}$, and A_i are projection matrices. The cosine-based gating function $\lambda_i(h_r)$ is defined as follows.

$$\lambda_i(h_r) = \begin{cases} \cos^a\left(\frac{d(h_i,h_r)}{w}\pi\right) & \text{if } d(h_i,h_r) < \frac{w}{2} \\ 0 & \text{else,} \end{cases} \quad (3)$$

where h_i is the heart phase in the i^{th} projection image, $w \in [0,1[$ controls the width and $a \geq 0$ controls the shape of the gating function. The distance between heart phases reads $d(h_1,h_2) = \min_{\varepsilon\in\{-1,0,1\}} |h_1 - h_2 + \varepsilon|$ [7]. Specifying optimal ECG-gating parameters w and a is challenging, as wider gating windows prevent undersampling but introduce motion artifacts into the reconstruction. Streak reduction is performed by omitting the N_{ign} smallest and largest contributions to each voxel. For a more comprehensive description of the algorithm refer to [6].

2) Dense motion field compensated reconstruction: Analytic expressions of the cardiac motion at the heart's surface are known for both the XCAT dynamics and the proposed twisting motion. Therefore, the 3D ground-truth deformation field can be incorporated directly into the reconstruction. However, the displacement vector fields are sparse, as they are defined only on the parametric surfaces of the phantom. For the use in motion-compensated reconstruction the sparse motion field is interpolated on a dense regular grid yielding an approximation of the true 3D cardiac motion $T^{(3D)}_{i,h_r}(\mathbf{x})$ [8]. The reconstruction is then calculated similarly to Eq. 2 omitting the streak reduction and the ECG-gating.

$$f_{h_r}(\mathbf{x}) = \sum_{i=1}^{N} \omega_i(\mathbf{x}') \cdot p_i\left(A_i(\mathbf{x}')\right), \quad (4)$$

where $\mathbf{x}' = T^{(3D)}_{i,h_r}(\mathbf{x})$.

C. Experimental Setup

All algorithms are implemented in CONRAD, an open-source simulation and reconstruction framework for cone-beam X-ray imaging [9]. We simulated a 4 s sweep acquiring 133 projections over 200° assuming a monochromatic source at 80 kV and a noise free process. The source-to-detector distance was 1200 mm and the source-to-isocenter distance was 800 mm. The detector had 620×480 pixels with an isotropic spacing of 0.616 mm. The reconstructed volumes had 256^3 voxels with an isotropic spacing of $1\,mm$.
The heart rate was chosen as 60 bpm resulting in a total of four heart cycles throughout the simulated acquisition. We simulated five different twist angles ranging from 0° to 30° ($\Phi^{\text{tot}} \in \{0°, 9°, 15°, 21°, 30°\}$). The intrinsic motion of the XCAT cardiac phantom was used to model contractive motion. Reconstructions were calculated at systole ($h_r = 0.5$) and at diastole ($h_r = 0.8$).
For the ECG-gated reconstruction described in Sec. II-B1 we chose $w = 0.4$, and $a = 4$ following [6]. Therefore,56 and 57 projections were used for the initial reconstruction of the fast and the quiet heat phase, respectively.
Streak reduction was performed using $N_{\text{ign}} = 3$.

D. Evaluation

We investigate the performance of ECG-gated cardiac vasculature reconstruction described in Section II-B1 and dense motion field compensated reconstruction (c.f. Section II-B2). The coronary arteries are of particular interest, as they are drastically affected by LV twist.
In the case of contrasted vasculature, quantitative evaluation was carried out using precision-recall (PR) curves. PR curves are calculated from the spatial overlap of a ground-truth volume $g(\mathbf{x})$ and a reconstructed volume $f^{(\alpha)}(\mathbf{x})$. The reconstruction is thresholded at increasingly restrictive levels α and then compared to the ground-truth. If an artery is present in $g(\mathbf{x})$ at $\mathbf{x}$ and also in $f^{(\alpha)}(\mathbf{x})$ $\mathbf{x}$ is called a true positive (TP), or a false negative (FN) if it is not present in $f^{(\alpha)}(\mathbf{x})$. However, if no artery exists in $g(\mathbf{x})$ while none is present in

$f^{(\alpha)}(\mathbf{x})$ $\mathbf{x}$ is a true negative (TN), else a false positive (FP). At each threshold α, the precision p and recall r are calculated.

$$p^{(\alpha)} = \frac{\mathrm{TP}^{(\alpha)}}{\mathrm{TP}^{(\alpha)} + \mathrm{FP}^{(\alpha)}}, \text{ and } r^{(\alpha)} = \frac{\mathrm{TP}^{(\alpha)}}{\mathrm{TP}^{(\alpha)} + \mathrm{FN}^{(\alpha)}}. \quad (5)$$

In order to efficiently compare different methods we use the area under the PR curve (AUPRC), reducing the measure to a single scalar value. As PR does not account for TP it may be favored over receiver operating characteristic when dealing with highly skewed datasets [10]. Similarly to the area under a receiver-operating curve, the optimal value for AUPRC is unity. Note however, that an AUPRC of 0.5 does not correspond to a random process.

In a second step we calculate the cross-correlation in a region-of-interest (ROI) of the reconstructed volumes with the ground-truth to assess overall reconstruction performance. The ROI γ was defined as an elliptical patch in the central slice of the volumes. The Pearson correlation coefficient reads

$$r = \frac{\sum_{\mathbf{x}} \left(f_\gamma(\mathbf{x}) - \bar{f}_\gamma\right) \left(g_\gamma(\mathbf{x}) - \bar{g}_\gamma\right)}{\sqrt{\sum_{\mathbf{x}} \left(f_\gamma(\mathbf{x}) - \bar{f}_\gamma\right)^2} \cdot \sqrt{\sum_{\mathbf{x}} \left(g_\gamma(\mathbf{x}) - \bar{g}_\gamma\right)^2}}, \quad (6)$$

where $\bar{f}_\gamma = \frac{1}{\sum_{\mathbf{x}} 1} \sum_{\mathbf{x}} f_\gamma(\mathbf{x})$, and $\mathbf{x} \in \gamma$ [11].

Both phase-resolved reconstruction methods described in Sections II-B1 and II-B2 were evaluated on a fast and a quiet heart phase ($h_r = 0.5$ and $h_r = 0.8$, respectively) at five different twist angles. LV twist was implemented according to Section II-A.

III. Results and Discussion

We present the results of our experiments evaluated using the AUPRC and the Pearson correlation coefficient (c.f. Section II-C and II-D). Tables I and II state the AUPRC for the coronary arteries and the Pearson correlation coefficient for overall performance calculated from the phase-resolved reconstructions and the ground-truth.

We found the AUPRC and the correlation to be largely constant at all twist angles. However, slight deteriorations of the AUPRC at $h_r = 0.5$ were observed at higher twist angles ($\Phi^{\mathrm{tot}} > 21°$) of the fast heart phase. This can likely be explained by gradually aggravating limited angle problems that are introduced with increasing cardiac torsion. The average angular increment over the 133 acquired projections was $1.50°$. Therefore, considering the twist motion model described in Section II-A, structures with twist angles of $24.98°$ would remain in phase during contraction. Rotation at the apex may therefore introduce limited angle problems during contraction, but not during relaxation. The contrary applies to the base due to the opposite rotation direction. It is worth mentioning that the AUPRC without any additional twist was also low for dense motion field compensated reconstruction at both reference heart phases. The same behavior was observed with the ECG-gated reconstruction at $h_r = 0.8$. We could not thoroughly eliminate other effects as possible reasons for the deterioration. Therefore, we have to be considerate with attributing deteriorations exclusively to cardiac twist.

ECG-gated:	Φ^{tot} in $°$	0	9	15	21	30
AUPRC	$h_r = 0.5$	0.201	0.201	0.203	0.190	0.195
	$h_r = 0.8$	0.296	0.317	0.314	0.310	0.309
Pearson r	$h_r = 0.5$	0.639	0.631	0.631	0.631	0.631
	$h_r = 0.8$	0.525	0.518	0.520	0.520	0.523

TABLE I
AUPRC and Pearson correlation coefficient for the ECG-gated reconstruction method using 57 of the 133 acquired projections at systole ($h_r = 0.5$) and at diastole $h_r = 0.8$ for five different twist angles ranging from $0°$ to $30°$.

Motion field:	Φ^{tot} in $°$	0	9	15	21	30
AUPRC	$h_r = 0.5$	0.189	0.202	0.194	0.190	0.176
	$h_r = 0.8$	0.185	0.204	0.199	0.196	0.194
Pearson r	$h_r = 0.5$	0.922	0.920	0.920	0.921	0.921
	$h_r = 0.8$	0.950	0.951	0.952	0.952	0.952

TABLE II
AUPRC and Pearson correlation coefficient obtained with the dense motion field compensated reconstruction at a fast and quiet heart phase (0.5 and 0.8, respectively) at five twist angles.

The AUPRC is substantially worse for dense motion field compensated reconstruction compared to ECG-gated reconstruction, $0.196 \pm 7.00 \cdot 10^{-3}$ compared to $0.309 \pm 8.00 \cdot 10^{-3}$ at $h_r = 0.8$. The streak reduction in the ECG-gated reconstruction suppressed high intensity artifacts, leading to an increased AUPRC. False positives at near optimal thresholds can be observed in the dense motion field reconstructions shown in Fig. 3b and 3e. As precision-recall is sensitive to false positives, the ECG-gated reconstruction scored better albeit missing smaller arteries (compare Fig. 3a, 3b, and 3c).

Moreover, the quality of the ECG-based reconstruction suffered at faster heart phases ($0.198 \pm 5.40 \cdot 10^{-3}$ and $0.309 \pm 8.00 \cdot 10^{-3}$ at $h_r = 0.5$ and 0.8, respectively) due to increased motion. The reconstruction quality achieved with dense motion field compensated reconstruction stayed mostly constant as expected, yielding $0.192 \pm 9.40 \cdot 10^{-3}$ and $0.196 \pm 7.00 \cdot 10^{-3}$ at $h_r = 0.5$ and 0.8, respectively.

In contrast to the AUPRC the Pearson correlation coefficient is sensitive to changed distributions in the data set. Therefore, values of r at different heart phases may not be compared due to changes in the heart's shape, illustrated in Fig. 4a and 4d. It is evident from Tables I and II that the dense motion field approach yielded significantly better results if the evaluation is not constrained to the coronary arteries. This is not surprising, because the ECG-gated reconstruction only incorporated 56 (57) projections for the reconstruction at systole (diastole). Decreasing performance due to limited angle problems was not observed using Pearson correlation coefficient, as other structures, such as the myocardium and cardiac chambers but also streak artifacts, dominated the image (see Fig. 4). Moreover, the appearance of those structures in X-ray imaging is only marginally affected by cardiac twist.

IV. Conclusion

We studied the effects of cardiac torsion on reconstruction quality in an interventional setting. The XCAT motion field

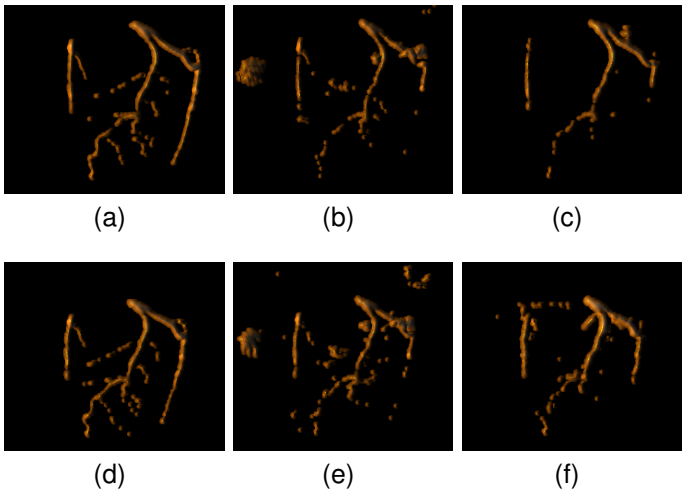

Fig. 3. Volume renderings of the reconstructed volumes shown in Fig. 4 at diastole (top) and systole (bottom) using appropriate thresholds: the ground-truth volume is shown in Fig. 3a and 3d, Fig. 3b and 3e show the dense motion field compensated reconstruction, and Fig. 3c and 3f show the ECG-gated reconstruction.

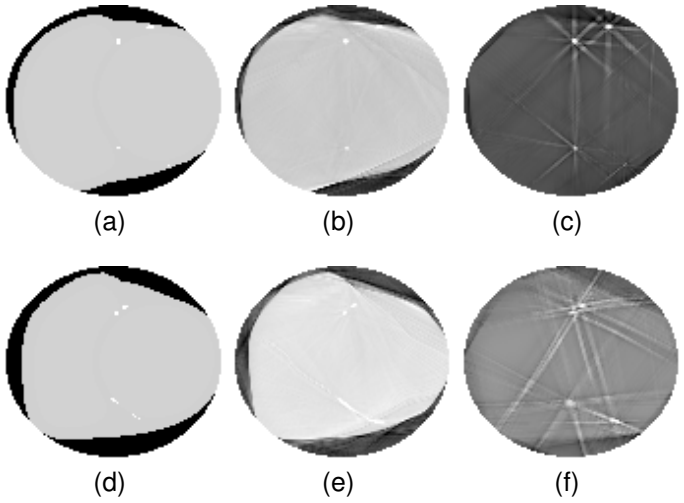

Fig. 4. ROI γ extracted from the ground-truth (Fig. 4a and 4d), dense motion field compensated reconstruction (Fig. 4b and 4e), and ECG-gated reconstruction (Fig. 4c and 4f) at $h_r = 0.8$ and 0.5 in the top and bottom row, respectively. Acquisitions without additional twist are shown.

was extended with an analytic motion model describing the wringing motion along the LV long axis. An ECG-gated reconstruction method and a dense motion field compensated algorithm were used to reconstruct volumes at systole and diastole at five twist angles. The reconstruction quality of the coronary arteries, which are particularly interesting as they follow cardiac twist, was assessed using the AUPRC. We found smaller values of the AUPRC for larger rotation angles, as they resulted in a per-projection twist motion close to the average angular increment of the acquisition and therefore introduced limited angle problems and streak artifacts. Overall reconstruction quality, assessed using Pearson's correlation coefficient in a central ROI, remained mostly constant.

Mean cardiac twist angles of $10.5° \pm 1.6°$ were observed in healthy volunteers [12] but values up to $21.1° \pm 15.2°$ were reported in pathologic cases [13]. In such cases, limited angle problems and therefore decreased reconstruction quality may occur in interventional settings. However, the initial results suggested that such effects are subtle and do not drastically affect the acquisitions.

ACKNOWLEDGMENT

The authors gratefully acknowledge funding of the Erlangen Graduate School in Advanced Optical Technologies (SAOT) in the framework of the German excellence initiative.

REFERENCES

[1] S. Nakatani, "Left ventricular rotation and twist: Why should we learn?" *Journal of Cardiovascular Ultrasound*, vol. 19, no. 1, pp. 1–6, 2011.

[2] E. Y. Sidky, C.-M. Kao, and X. Pan, "Accurate image reconstruction from few-views and limited-angle data in divergent-beam ct," *Journal of X-ray Science and Technology*, vol. 14, no. 2, pp. 119–139, 2006.

[3] W. Segars, M. Mahesh, T. Beck, E. Frey, and B. Tsui, "Realistic ct simulation using the 4d xcat phantom," *Medical physics*, vol. 35, no. 8, pp. 3800–3808, 2008.

[4] A. Maier, H. G. Hofmann, C. Schwemmer, J. Hornegger, A. Keil, and R. Fahrig, "Fast simulation of x-ray projections of spline-based surfaces using an append buffer," *Physics in medicine and biology*, vol. 57, no. 19, p. 6193, 2012.

[5] Y. Notomi, R. M. Setser, T. Shiota, M. G. Martin-Miklovic, J. Weaver, Z. B. Popovic, H. Yamada, N. L. Greenberg, R. D. White, and J. D. Thomas, "Assessment of left ventricular torsional deformation by doppler tissue imaging validation study with tagged magnetic resonance imaging," *Circulation*, vol. 111, no. 9, pp. 1141–1147, 2005.

[6] C. Schwemmer, C. Rohkohl, G. Lauritsch, K. Müller, and J. Hornegger, "Residual motion compensation in ecg-gated cardiac vasculature reconstruction," in *Proceedings of the Second International Conference on Image Formation in X-ray Computed Tomography, edited by Noo F.(University of Utah, Salt Lake City, Utah, 2012)*, 2012, pp. 259–262.

[7] C. Rohkohl, G. Lauritsch, A. Nottling, M. PrUmmer, and J. Hornegger, "C-arm ct: Reconstruction of dynamic high contrast objects applied to the coronary sinus," in *Nuclear Science Symposium Conference Record, 2008. NSS'08. IEEE*. IEEE, 2008, pp. 5113–5120.

[8] A. Maier, O. Taubmann, J. Wetzl, J. Wasza, C. Forman, P. Fischer, J. Hornegger, and R. Fahrig, "Fast interpolation of dense motion fields from synthetic phantoms," in *Bildverarbeitung für die Medizin 2014*. Springer, 2014, pp. 168–173.

[9] A. Maier, H. G. Hofmann, M. Berger, P. Fischer, C. Schwemmer, H. Wu, K. Mueller, J. Hornegger, J. H. Choi, C. Riess, A. Keil, and R. Fahrig, "CONRAD - A software framework for cone-beam imaging in radiology," *Medical Physics*, vol. 40, no. 11, pp. 111 914–1–8, 2013.

[10] J. Davis and M. Goadrich, "The relationship between precision-recall and roc curves," in *Proceedings of the 23rd international conference on Machine learning*. ACM, 2006, pp. 233–240.

[11] J. Martin Bland and D. Altman, "Statistical methods for assessing agreement between two methods of clinical measurement," *The lancet*, vol. 327, no. 8476, pp. 307–310, 1986.

[12] F. Carreras, J. Garcia-Barnes, D. Gil, S. Pujadas, C. H. Li, R. Suarez-Arias, R. Leta, X. Alomar, M. Ballester, and G. Pons-Llado, "Left ventricular torsion and longitudinal shortening: two fundamental components of myocardial mechanics assessed by tagged cine-mri in normal subjects," *The international journal of cardiovascular imaging*, vol. 28, no. 2, pp. 273–284, 2012.

[13] S. M. Shaw, D. J. Fox, and S. G. Williams, "The development of left ventricular torsion and its clinical relevance," *International Journal of Cardiology*, vol. 130, no. 3, pp. 319 – 325, 2008. [Online]. Available: http://www.sciencedirect.com/science/article/pii/S0167527308007006